Arthritis & Rheumatology
Vol. 78, No. 4, April 2026, pp 880–895
DOI 10.1002/art.43434

American College of Rheumatology
Empowering Rheumatology Professionals

Identification of Histone Deacetylase Inhibitor Targeting Type I Interferon and B Cell Abnormalities in Systemic Lupus Erythematosus

Takehiro Hirayama,[1,2] Hachiro Konaka,[1,3] Yasuhiro Kato,[1,2,4] Takayuki Shibahara,[1,5] Chisato Nishizawa,[6,7] Kohei Tsujimoto,[1,2,4] JeongHoon Park,[1] Eri Itotagawa,[1,2] Tatsunori Jo,[1,2] Masayuki Nishide,[1,2,4] Sumiyuki Nishida,[1,8,9] Yoshihito Shima,[1,10] Masashi Narazaki,[1,4] Wataru Aoki,[6,7] Ken J Ishii,[11] Hyota Takamatsu,[1,12] and Atsushi Kumanogoh[1,2,4,13,14]

Objective. Systemic lupus erythematosus (SLE) is characterized by increased Type I interferon (IFN-I) and autoantibody production. This study aimed to identify drugs that can inhibit both IFN-I and autoantibody production.

Methods. We identified an inhibitor of IFN-I production from a chemical library. Subsequently, we examined its efficacy and underlying mechanisms in suppressing the expression and phosphorylation of upstream signaling molecules for IFN-I production and the differentiation of B cells into plasma cells. Additionally, we examined whether it could alleviate disease severity in SLE-prone mice.

Results. We showed that vorinostat, a clinically approved pan-histone deacetylase (HDAC) inhibitor, inhibited both IFN-I production and plasma cell differentiation. Vorinostat suppressed IFN-I production by inhibiting TBK1 phosphorylation and the subsequent IRF3 nuclear translocation and suppressed plasma cell differentiation by inhibiting the expression of essential transcriptional factors for plasma cells. Notably, inhibiting HDAC6 suppressed IFN-I induction and plasma cell differentiation. Furthermore, vorinostat ameliorated lung inflammation in STING-associated vasculopathy with onset in infancy mice by decreasing IFN-I and alleviated the mortality and severity of renal disease in New Zealand Black/White F1 mice by suppressing IFN-I induction and B cell differentiation.

Conclusion. Vorinostat ameliorates the severity of disease in SLE-prone mice by simultaneously suppressing IFN-I production and plasma cell differentiation by targeting HDAC6. Thus, vorinostat is a promising therapeutic agent for SLE and may benefit patients with SLE requiring more effective and better-tolerated therapies.

Supported in part by the Japan Science and Technology Agency (JST; grant JPMJSP2138 to Dr Hirayama), Japan Society for the Promotion of Science (JSPS) KAKENHI (grant 22H03111 to Dr Takamatsu, grant JP18H05282 to Dr Kumanogoh, and grant 18K08386), a Core Research for Evolutionary Science and Technology (CREST) grant from JST (grant JPMJCR16G2 to Dr Takamatsu), the Center of Innovation program (COI-STREAM) from the Ministry of Education, Culture, Sports, Science and Technology (MEXT), Japan (to Dr Kumanogoh), the Japan Agency for Medical Research and Development (AMED)-CREST (grant 15652237 to Dr Kumanogoh), AMED (grant 23gm4010022h0001 to Dr Takamatsu, grant JP18cm059042 to Dr Kumanogoh, and grants J200705023, J200705710, J200705049, and JP18cm016335), and grants from The Mitsubishi Foundation (to Dr Kumanogoh).

[1]Department of Respiratory Medicine and Clinical Immunology, Graduate School of Medicine, Osaka University, Osaka, Japan; [2]Department of Immunopathology, Immunology Frontier Research Center, Osaka University, Osaka, Japan; [3]Department of Internal Medicine, Nippon Life Hospital, Osaka, Japan; [4]Department of Advanced Clinical and Translational Immunology, Graduate School of Medicine, Osaka University, Osaka, Japan; [5]Department of Internal Medicine, Daini Osaka Police Hospital, Osaka, Japan; [6]Division of Applied Life Sciences, Graduate School of Agriculture, Kyoto University, Kyoto, Japan; [7]Department of Biotechnology, Graduate School of Engineering, Osaka University, Osaka, Japan; [8]Strategic Global Partnership & X (Cross)-Innovation Initiative Graduate School of Medicine, Osaka University and Osaka University Hospital, Osaka, Japan; [9]Center for Advanced Modalities and Drug Delivery System, Osaka University, Osaka, Japan; [10]Laboratory of Thermo-Therapeutics for Vascular Dysfunction, Graduate School of Medicine, Osaka University, Osaka, Japan; [11]Division of Vaccine Science, Department of Microbiology and Immunology, The Institute of Medical Science, The University of Tokyo, Tokyo, Japan; [12]Department of Clinical Research Center, National Hospital Organization Osaka Minami Medical Center, Osaka, Japan; [13]Center for Infectious Disease for Education and Research, Osaka University, Osaka, Japan; [14]Integrated Frontier Research for Medical Science Division, Institute for Open and Transdisciplinary Research Initiatives, Osaka University, Osaka, Japan.

Additional supplementary information cited in this article can be found online in the Supporting Information section (https://acrjournals.onlinelibrary.wiley.com/doi/10.1002/art.43434).

Author disclosures are available at https://onlinelibrary.wiley.com/doi/10.1002/art.43434.

Address correspondence via email to Hyota Takamatsu, MD, PhD, at thyota@imed3.med.osaka-u.ac.jp.

Submitted for publication May 27, 2024; accepted in revised form October 6, 2025.

INTRODUCTION

Systemic lupus erythematosus (SLE) is an autoimmune disease characterized by the production of autoantibodies against various autoantigens, including nucleic acids and interacting proteins, resulting in inflammation and tissue damage.[1] This systemic immune response results in life-threatening complications such as severe lupus nephritis, neuropsychiatric symptoms, and hematologic abnormalities, causing chronic organ damage and death. Immunosuppressive therapy with high-dose glucocorticoids and cyclophosphamide is commonly used during the acute and relapsing phases of SLE to decrease disease activity; however, this increases infection risk. Therefore, developing therapies that specifically inhibit aggravating factors modulating SLE pathogenesis is necessary. Evidence suggests that overproduction of Type I interferon (IFN-I) and aberrant B cell differentiation[2,3] are involved in SLE pathogenesis. Recently, biologics specifically targeting the IFN-I receptor (anifrolumab) and B cell–activating factor (BAFF; belimumab) have been approved for some patients with SLE. SLE stratification has been proposed to clarify patient characteristics responsive to these drugs. In the chronic phase, patients with SLE are classified into two groups by their clinical manifestations: the IFN- and lymphocyte-associated groups.[4] However, in the acute or relapsing stages of SLE, a pronounced increase in IFN-I production and pathologic B cell proliferation are observed.[5]

Several pathways involving IFN-I production play a pivotal role in SLE pathogenesis.[1,6] For instance, the Toll-like receptor 7 (TLR7)–MyD88-dependent pathway, the RIG-I-MAVS–mediated pathway, and the cGAS-STING pathway promote TBK1 activation, leading to the nuclear translocation[7] of IRF3 and IRF7. Previous studies have identified several disease susceptibility genes related to IFN-I–inducing pathways, such as *IRF5*, *STAT4*, and *TLR7*, in SLE. For instance, IRF5 is involved in increased IFN-I production by plasmacytoid dendritic cells (pDCs) via TLR7–9 stimulation.[8–10] Activation of TLR7 by immune complexes containing autologous RNA causes IFN-I overproduction by pDCs.[11] Therefore, inhibiting IFN-I induction by targeting shared pathways such as TBK1 may be effective for SLE treatment.

The differentiation of B cells to plasma cells (PCs) is tightly regulated by key transcription factors,[12] including *Prdm1* (encoding Blimp-1), *XBP1*, and *IRF4*. *Prdm1* acts as a master regulator of PC differentiation, whereas *XBP1* is essential for Ig secretion and the unfolded protein response in PCs.[13] *IRF4* coordinates with these factors to drive the PC program.[14] Under pathologic conditions, B cells differentiate outside the germinal center into short-lived plasmablasts through activated naive B cells, double-negative B cells (DNBs), and unswitched memory B cells.[15] DNBs are a unique B cell subset involved in autoimmune diseases such as SLE[10] and corresponds to mouse age-associated B cells (ABCs).[16,17] DNBs and ABCs, expressing T-bet and CD11c, are developed via TLR7 signaling with B cell receptor (BCR) signaling and cytokines, such as interleukin 21 (IL-21) and IFN-γ. Therefore, targeting TLR7 downstream signaling molecules may be beneficial in simultaneously suppressing IFN-I production and pathologic B cell maturation.

In this study, we screened an inhibitor of IFN-I production from a chemical library of clinically approved drugs and identified vorinostat, a pan-histone deacetylase (HDAC) inhibitor targeting HDAC1, HDAC2, HDAC3, and HDAC6, and a clinically approved drug for cutaneous T cell lymphoma.[18] Subsequently, we examined whether vorinostat suppresses the expression and phosphorylation of upstream signaling molecules for IFN-I and the differentiation of B cells into PCs. Furthermore, we elucidated which HDAC isoform is involved in its therapeutic effect using HDAC isoform–specific inhibitors. We also examined whether vorinostat could alleviate disease severity in SLE-prone mice, including STING-associated vasculopathy with onset in infancy (SAVI) mice and New Zealand Black/White F1 (NZB/W F1) mice.

MATERIALS AND METHODS

Clinical samples. Participants were Japanese patients admitted to the Department of Clinical Immunology at Osaka University from 2015 to 2024. Patients with SLE were diagnosed based on the 1997 American College of Rheumatology revised criteria for the classification of SLE.[19] Healthy control samples were obtained from six volunteer donors. The enrollment of human participants was approved by the ethical review boards of Osaka University (12456 and 11122) and is in accordance with the Declaration of Helsinki. Informed consent was obtained from the participants.

Mice. C57BL/6 mice were purchased from CLEA Japan (Tokyo, Japan), and NZB/W F1 female mice were obtained from Japan SLC (Hamamatsu, Japan). SAVI N153S KI mice, developed by Prof Masahiro Yamamoto, were kindly provided by Prof Ken J. Ishii. Heterozygous SAVI mice were used because homozygous SAVI is lethal.[20,21] Mice were housed in pathogen-free facilities at the Faculty of Medicine at Osaka University and fed a standard diet and water. The animal experiment protocol was approved by the Faculty of Medicine at Osaka University (02-093-009), and all experiments were conducted in accordance with the Institute of Experimental Animal Sciences' policies.

Drug screening. THP1-Blue ISG cells purchased from InvivoGen (San Diego, CA) and peripheral blood mononuclear cells (PBMCs) were seeded and treated with compounds from the Prestwick Chemical Library (Prestwick Chemical, San Diego, CA) at 1 μM in the presence of resiquimod (R848; 10 μg/mL), 2'3'-cyclic GMP-AMP (2'3'-cGAMP; 5 μg/mL), or IFN-I (Universal IFN-I; 200 U/mL) for 24 hours. Universal IFN-I was used with the expectation of IFN-αA activity, confirmed in our previous experiments to exhibit stable effects. IFN-I production was

evaluated using HEK-Blue IFN-α/β, HEK-Blue TNF-α, HEK-Blue IL-6, and B16-Blue IFN-α/β reporter cells (InvivoGen) as previously described,[1] and cell viability was measured using the cell counting kit-8 (Dojindo Laboratories, Tokyo, Japan). The inhibitory effects of the compounds were calculated by dividing the ratio of the cell counting kit-8 assay values (compound-treated cells/control cells) by the ratio of the secreted embryonic alkaline phosphatase (SEAP) assay values (compound-treated cells/control cells).

In vitro IFN-I production assay. To evaluate vorinostat inhibitory effect on IFN-I production, THP1-Blue ISG cells were seeded in 96-well plates at a density of 1 × 105 cells/well and treated with vorinostat (1, 10, or 100 μM). Cells were stimulated with lipopolysaccharide (LPS; 500 ng/mL), 2'3'-cGAMP (5 μg/mL), or R848 (5 μg/mL) for 24 hours. Supernatants were then collected, and the QUANTI-Blue assay (InvivoGen, San Diego, CA) was performed according to the manufacturer's instructions. To evaluate the inhibitory effect of vorinostat on IFN-I production in primary cells, PBMCs were seeded at 1 × 105 cells/well and treated with vorinostat (1, 10, or 100 μM). The cells were then stimulated with LPS (500 ng/mL), 2'3'-cGAMP (5 μg/mL), or R848 (5 μg/mL) for 24 hours. Following stimulation, the supernatants were collected, and IFN-I activity was evaluated using a reporter assay with HEK-Blue IFN-α/β cells.

Western blotting and fluorescence imaging. Phorbol myristate acetate (PMA)–treated THP1 cells were stimulated with 2'3'-cGAMP for four hours with or without vorinostat. Subsequently, cells were fixed with 4% paraformaldehyde, permeabilized with 0.1% Triton X-100, blocked with Blocking One Histo (Nacalai Tesque, Kyoto, Japan), and stained with primary antibody against IRF3 (1:500) at 4°C overnight. After washing, cells were stained with Alexa Fluor 488–conjugated anti-rabbit IgG (1:1000) and DAPI (1:2000) for one hour. The nuclear translocation rate was defined as the ratio of Alexa Fluor 488 fluorescence intensity within the DAPI-positive nucleus to the total cellular Alexa Fluor 488 fluorescence intensity. Multiple fields were imaged using a Keyence BZ-X800 microscope, and the nuclear translocation rate was quantified.

RNA-sequencing analysis. Total RNA was isolated from THP1-Blue ISG cells stimulated with LPS (500 ng/mL) or 2'3'-cGAMP (5 μg/mL) in the presence or absence of vorinostat (10 μM) using the FastGene RNA Premium Kit (NIPPON Genetics, Tokyo, Japan) according to the manufacturer's instructions. RNA quality was assessed using the Bioanalyzer RNA Nano (Agilent Technologies, Santa Clara, CA). Libraries were prepared using the TruSeq Stranded messenger RNA (mRNA) Library Prep Kit (Illumina, San Diego, CA) and sequenced on the Illumina NovaSeq 6000 platform. Raw reads were aligned to the human reference genome (hg38) using TopHat (version 2.1.1), and gene expression levels were quantified using Cufflinks (version 2.2.1). Differential expression analysis and pathway enrichment analysis were performed using integrated Differential Expression and Pathway analysis (iDEP.96),[22] and molecular network analysis was conducted using Ingenuity Pathway Analysis (QIAGEN).

Quantitative real-time polymerase chain reaction analyses. For isolation of RNA from mouse kidney, lung, and spleen tissues, the samples were homogenized using zirconia beads and the Tissue Lyser II (QIAGEN, Venlo, the Netherlands). RNA was then extracted using QIAzol Lysis Reagent (QIAGEN) and chloroform according to the manufacturer's instructions. After chloroform extraction, the mouse samples were further processed using the FastGene RNA Premium Kit (NIPPON Genetics) following the manufacturer's protocol. RNA from human B cells was isolated using the same FastGene RNA Premium Kit. RNA concentration and purity were determined using NanoDrop Technology (Thermo Fisher Scientific, Wilmington, DE). Complementary DNA synthesis was performed using the PrimeScript RT Reagent Kit (Takara Bio, Shiga, Japan) following the manufacturer's protocol. Quantitative real-time polymerase chain reaction (PCR) was conducted using the QuantStudio 7 instrument (Thermo Fisher Scientific) with TaqMan Gene Expression Assays (Thermo Fisher Scientific) (Supplementary Materials). The PCRs were set up according to the manufacturer's guidelines, and the relative gene expression was calculated using the standard curve method, with *ACTB* (β-actin) as the endogenous control.

In vitro B cell differentiation assay. B cells were isolated from PBMCs of healthy donors and patients with SLE using the EasySep Human B Cell Enrichment Kit II without CD43 depletion (STEMCELL Technologies, Vancouver, BC, Canada). B cells were stimulated in RPMI with 10% fetal bovine serum supplemented with nonessential amino acids, glutamine, sodium pyruvate, Primocin (InvivoGen), R848 (1 μg/mL), BAFF (10 ng/mL), IL-21 (10 ng/mL), IL-2 (50 U/mL), IFN-γ (20 ng/mL), and goat F(ab)'2 anti-human IgG (10 μg/mL). Cells were treated with or without vorinostat (0.25, 0.5, 1, or 2 μM) and anifrolumab (5, 10, 25, or 50 μg/mL) for three days. After three days, cells were washed and resuspended in fresh media containing R848 and cytokines, with or without vorinostat and anifrolumab, but without anti-IgG and IgM. Cells were cultured for an additional 4 or 7 days (7 or 10 days in total) before use in subsequent assays.

Flow cytometry. For mice, cells were blocked with anti-mouse CD16/32 (category 101302; BioLegend, San Diego, CA) and stained with the fluorochrome-conjugated antibodies described in Supplementary Materials and Reagents. Splenic pDCs were defined as B220+PDCA1+ cells. Splenic B cells were defined as B220+ cells, immature B cells were defined as B220+IgM+IgD– cells, and mature B cells were defined as B220+IgM–IgD+ cells. ABCs were defined as CD4–CD8–NK1.1

–B220+T-bet+CD11c+ cells. Bone marrow cells were lineage-negative (Lin–), defined as CD4–CD8–NK1.1–CD3–CD11b–CD11c–. Pro-B cells were defined as Lin–c-kit+B220–CD43+ cells, and pre-B cells were defined as Lin–c-kit–B220+CD25+ cells. For human samples, B cells were isolated from PBMCs of healthy donors and patients with SLE using the EasySep Human B Cell Enrichment Kit II without CD43 Depletion (STEMCELL Technologies), according to the manufacturer's instructions. Subsequently, B cells were blocked with FcR Blocking Reagent human (Miltenyi Biotec, Bergisch Gladbach, Germany) and stained with the fluorochrome-conjugated antibodies described in Supplementary Table S1. Plasma blasts were defined as CD19+CD27+CD38+ CD138– cells, and PCs were identified as CD19+CD27+CD38+CD138+ cells. All cell populations were analyzed after the exclusion of doublets and dead cells. Samples were analyzed using a BD FACS Canto II or BD FACS Symphony A1 flow cytometer (BD Biosciences). Flow cytometry data were analyzed with FlowJo software (BD Biosciences).

In vivo vorinostat administration in lupus-prone mice. For the murine hyper IFN-I–related disease model, 8- to 10-week-old SAVI mice were intraperitoneally administered vorinostat (20 mg/kg) or solvent (DMSO) daily for eight weeks. Next, urine samples were collected. Mice were euthanized by CO_2 inhalation, followed by the collection of blood, lung, and kidney tissues. For the murine lupus model, female NZB/W F1 mice (n = 18 per group) were randomly assigned to either the vehicle control or vorinostat treatment group at 22 weeks of age. Vorinostat (20 mg/kg) or an equivalent volume of vehicle was administered intraperitoneally five times per week for 16 weeks. To evaluate the short-term effects of vorinostat in vivo, an additional cohort of 25-week-old female NZB/W F1 mice (n = 9 per group) was treated with high-dose vorinostat (40 mg/kg body weight) or vehicle daily for four weeks. At the end of the treatment, mice were euthanized, and blood was collected by cardiac puncture. Serum was collected using standard procedures and stored at –80°C until use. Spleen, kidney, and bone marrow tissues were processed for flow cytometry, histology, and gene expression analyses, as described in the respective sections.

Measurement of in vivo vorinostat concentration. Female C57BL/6J mice (8 weeks old) received a single intraperitoneal injection of vorinostat (20 mg/kg). At designated time points (15 minutes, 1 hour, 2 hours, 4 hours, 8 hours, and 24 hours) after administration, mice were euthanized by CO_2 inhalation. Blood was collected by cardiac puncture, and the liver and spleen were immediately harvested. Vorinostat was extracted by adding 80% acetonitrile. The extracted samples were analyzed using a nano liquid chromatography mass spectrometry system (UltiMate 3000 RSLCnano and Orbitrap Exploris 240) equipped with an InertCore Plus C18 column (GL Sciences, Tokyo, Japan). A gradient was produced by changing the mixing ratio of the two eluents: A, 0.1% (volume/volume) formic acid, and B, acetonitrile. The gradient started with 10% B with a two-minute hold, was then increased to 50% B for five minutes, and finally increased to 95% B for a three-minute hold, after which the mobile phase was returned to its initial composition and held for two minutes to re-equilibrate the column. The autosampler and column oven were maintained at 4°C and 40°C, respectively. Vorinostat was detected in the positive mode followed by multiple reaction monitoring at a resolution of 15,000. The Electrospray Ionization (ESI) voltage and normalized collision energy were 3.5 kV and 30%, respectively. The heated ESI interface temperature and vaporizer temperature were 320°C and 275°C, respectively. The single-protonated precursor ion and product ion corresponding to vorinostat were 265 m/z and 232 m/z, respectively.

Evaluation of proteinuria. Proteinuria was assessed semiquantitatively using urine test strips (Siemens Healthcare Diagnostics, Deerfield, IL) and scored as follows: 0, negative; 1+, 30 mg/dL; 2+, 100 mg/dL; 3+, 300 mg/dL; and 4+, ≥1,000 mg/dL.

Immunohistochemical analysis. Kidneys were embedded in Tissue-TekVR optimal cutting temperature compound (OCT; Sakura Finetek, Torrance, CA). Frozen OCT samples were sectioned and affixed to glass slides. They were then warmed to room temperature, dried for 30 minutes, and fixed in cold acetone (–20°C) at room temperature for 10 minutes. After washing in phosphate-buffered saline (PBS), slides were blocked with PBS containing 1% bovine serum albumin for 60 minutes at room temperature. Slides were then incubated with a mixture of antibodies, tetramethylrhodamine-conjugated goat anti-mouse IgG, fluorescein isothiocyanate–conjugated donkey anti-mouse IgM (Jackson ImmunoResearch, West Grove, PA), and rat monoclonal antibody to C3 (Abcam, Cambridge, United Kingdom) for 12 hours at 4°C in a dark humid box. After washing with PBS, slides were incubated with the secondary antibody of Alexa Fluor 647 donkey anti-rat IgG (Invitrogen) for 1 hour at room temperature. Slides were mounted with DAPI (BioLegend) and imaged with an FV-3000 (Olympus, Tokyo, Japan).

Histopathological analysis. To perform lung histology, lungs were extracted and fixed with 4% paraformaldehyde. The tissues were embedded in paraffin and stained with hematoxylin and eosin. Lung pathologic changes were observed using an optical microscope. Histologic scoring parameters included edema, intra-alveolar cellular infiltration, congestion, and alveolar hemorrhage. The scores for each item were recorded on one of four levels[23]: normal (0), mild (1), moderate (2), and severe (3). The pathologic changes in the kidneys were assessed by evaluating glomerular activity, including glomerular proliferation, karyorrhexis and/or fibrinoid necrosis, cellular crescents, hyaline

deposits, and inflammatory cells. Sections were scored using a 0 to 3 scale for glomerular activity, where 0 indicated no lesions, 1 indicated lesions in <25% of glomeruli, 2 indicated lesions in 25% to 50% of glomeruli, and 3 indicated lesions in >50% of glomeruli. The mean scores for individual pathologic features were summed to obtain the glomerular activity score.[24]

Statistical analyses. Data are reported as mean ± SEM. Statistical significance was analyzed with the unpaired Mann–Whitney test using Prism software (GraphPad, San Diego, CA). Statistical significance is represented by the following notation: $^{*}P < 0.05$, $^{**}P < 0.01$, $^{***}P < 0.001$, and $^{****}P < 0.0001$.

Reporting patient and public involvement in research. Patients were enrolled through the provision of clinical samples. These samples were concurrently collected with the study and used to validate findings obtained from preclinical experiments and animal models. Data are available from the corresponding author upon request.

RESULTS

Identification and characterization of vorinostat in inhibiting IFN-I production. As shown in Figure 1A, we first screened therapeutic compounds capable of targeting both IFN-I production and B cell abnormalities in SLE using the Prestwick Chemical Library, which consists of clinically approved drugs. THP1-Blue ISG cells (a monocytic cell line engineered to monitor IFN-I signaling through SEAP reporter activity) were stimulated with IFN-α and 2'3'-cGAMP, a STING ligand, in the presence of these compounds. Human PBMCs were also stimulated with R848, a TLR7 ligand, because of the lower expression of TLR7 in THP1 cells. Regardless of cell type and ligands, vorinostat was among the top 20 candidate drugs that effectively suppressed IFN-I production while maintaining survival (Figure 1B and 1C). We selected vorinostat for this study because it has also been reported to regulate lymphocyte differentiation and proliferation via chromatin remodeling and confirmed its inhibitory effect on IFN-I production. THP1-Blue ISG cells or PBMCs were stimulated with LPS, 2'3'-cGAMP, and R848 with or without vorinostat. Vorinostat suppressed ISG induction in THP1-ISG cells and IFN-I production in PBMCs (Figure 1D and 1E). Notably, vorinostat suppressed IFN-I production in primary immune cells such as pDCs and monocytes (Supplementary Figure S1A). We then performed RNA-sequencing (RNA-seq) analysis to identify gene alterations upon LPS or cGAMP stimulation in the presence or absence of vorinostat. Both IFN-I– and B cell–related genes upregulated upon LPS or 2'3'-cGAMP stimulation were downregulated by vorinostat treatment (Supplementary Figure S1B). Ingenuity Pathway Analysis using RNA-seq data revealed interrelationships among genes inhibited by vorinostat, including cGAS, TLR7, IRF, and STAT1 in the network (Supplementary Figure S1C).

Gene Set Enrichment Analysis demonstrated significant enrichment in pathways related to IFN-I and adaptive immunity (Supplementary Figure S1D; Supplementary Tables S1 and S2). Further evaluation of IFN-I– and NF-κB–related genes revealed that vorinostat preferentially suppressed IFN-related genes compared to NF-κB pathway–related genes (Supplementary Table S3). Furthermore, although vorinostat exhibited broad suppressive effects on IFN-related genes such as *IFNB1*, *Mx1*, and *IRF7*, *IRF3* expression remained unchanged (Supplementary Figure S1E). Additionally, the degree of inhibition by vorinostat differed depending on the molecule in NF-κB–related genes that were induced more by LPS than that by cGAMP (Supplementary Table S4). Moreover, the expression of genes related to metabolism and cell cycle regulation also changed. For example, the expression of major glycolytic enzymes such as *LDHA* and *FBP1* was significantly decreased, whereas the expression of tricarboxylic acid cycle–related genes was almost unaffected. In addition, the expression of multiple mitotic checkpoint regulators, including *KNL1* and *APC/C*, was decreased (Supplementary Figure S2). On the other hand, no off-target pathway was observed in human PBMCs by vorinostat in the steady-state condition. These results suggest that vorinostat preferentially downregulates the expression of IFN-I–related genes involved in TLR-MyD88 and cGAS-STING pathways.

Vorinostat suppresses IFN-I expression by reducing the phosphorylation of TBK1. TBK1 phosphorylation and subsequent IRF3 nuclear translocation via TLR-MyD88 and cGAS-STING pathways induce IFN-I.[25,26] Therefore, we hypothesized that vorinostat might suppress IFN-I production by inhibiting TBK1 and IRF3 phosphorylation upon stimulation with LPS or 2'3'-cGAMP.[27] When THP1 cells were stimulated with LPS or cGAMP, the phosphorylation of TBK1 and IRF3 decreased with vorinostat treatment (Figure 2A). Immunofluorescence staining showed that IRF3 nuclear translocation induced by cGAMP stimulation was reduced by vorinostat (Figure 2B and 2C). Moreover, IFN-I production is regulated by other IRFs, including IRF5, IRF7, and IRF9. We found that the expression of IRF5, IRF7, and IRF9 was down-regulated by vorinostat treatment (Figure 2D). Consistently, quantitative PCR analysis confirmed that vorinostat treatment suppressed the expression of IFN-I–related genes, such as *IRF7*, *Ifi27*, *TMEM173*, and *IFN-β*, whereas *IRF3* expression remained unchanged (Figure 2E). Notably, when we compared the half-maximal inhibitory concentration values of vorinostat for suppressing IFN-I, TNF, IL-1β, and IL-6 production in LPS-stimulated PBMCs, vorinostat inhibited IFN-I production at a lower concentration compared with other cytokines (Figure 2F). These results indicate that vorinostat inhibits IFN-I production by suppressing TBK1 phosphorylation and the downstream signaling pathway, as well as the expression of IRF family transcription factors.

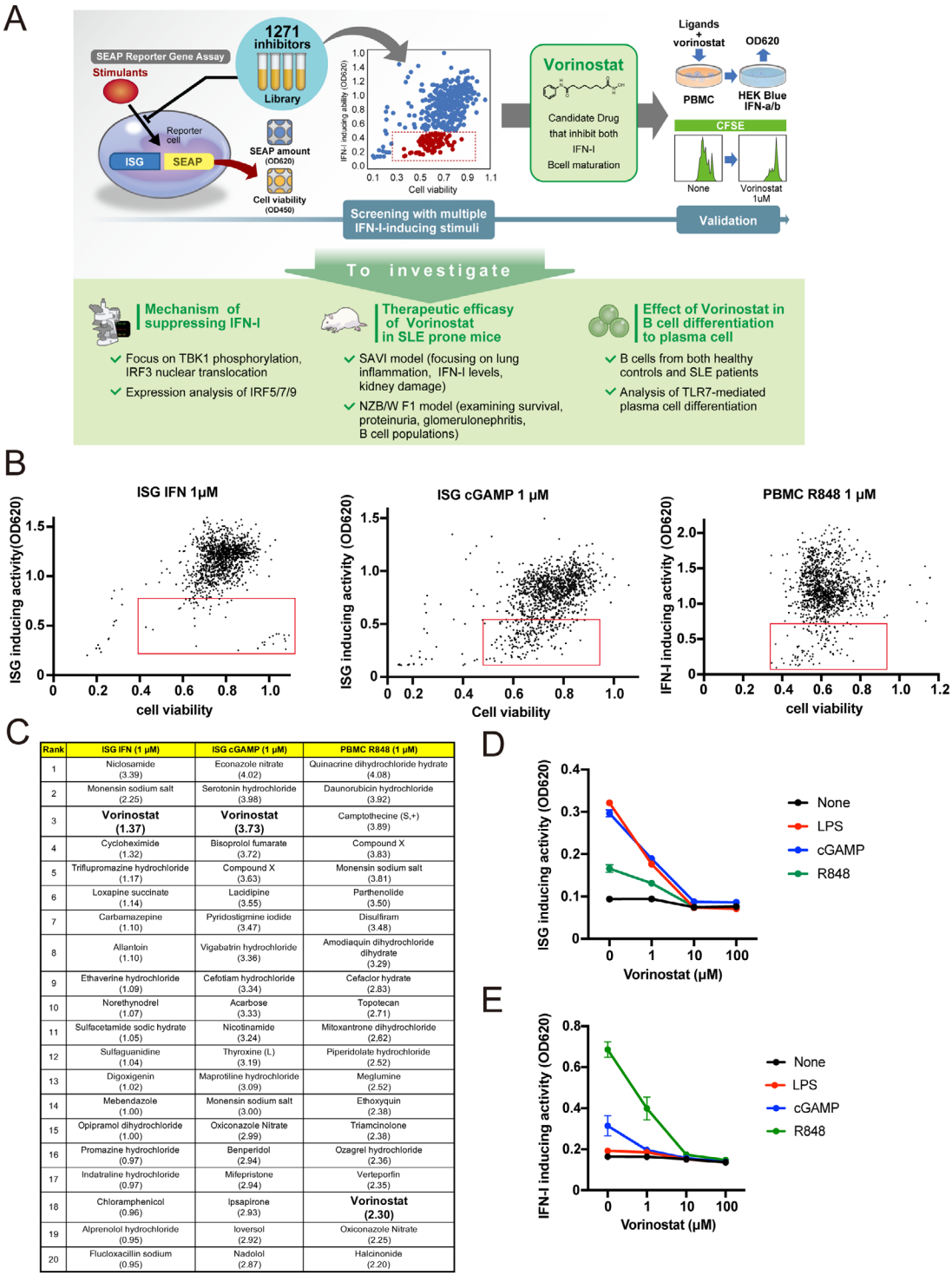

Rank	ISG IFN (1 μM)	ISG cGAMP (1 μM)	PBMC R848 (1 μM)
1	Niclosamide (3.39)	Econazole nitrate (4.02)	Quinacrine dihydrochloride hydrate (4.08)
2	Monensin sodium salt (2.25)	Serotonin hydrochloride (3.98)	Daunorubicin hydrochloride (3.92)
3	**Vorinostat (1.37)**	**Vorinostat (3.73)**	Camptothecine (S,+) (3.89)
4	Cycloheximide (1.32)	Bisoprolol fumarate (3.72)	Compound X (3.83)
5	Triflupromazine hydrochloride (1.17)	Compound X (3.63)	Monensin sodium salt (3.81)
6	Loxapine succinate (1.14)	Lacidipine (3.55)	Parthenolide (3.50)
7	Carbamazepine (1.10)	Pyridostigmine iodide (3.47)	Disulfiram (3.48)
8	Allantoin (1.10)	Vigabatrin hydrochloride (3.36)	Amodiaquin dihydrochloride dihydrate (3.29)
9	Ethaverine hydrochloride (1.09)	Cefotiam hydrochloride (3.34)	Cefaclor hydrate (2.83)
10	Norethynodrel (1.07)	Acarbose (3.33)	Topotecan (2.71)
11	Sulfacetamide sodic hydrate (1.05)	Nicotinamide (3.24)	Mitoxantrone dihydrochloride (2.62)
12	Sulfaguanidine (1.04)	Thyroxine (L) (3.19)	Piperidolate hydrochloride (2.52)
13	Digoxigenin (1.02)	Maprotiline hydrochloride (3.09)	Meglumine (2.52)
14	Mebendazole (1.00)	Monensin sodium salt (3.00)	Ethoxyquin (2.38)
15	Opipramol dihydrochloride (1.00)	Oxiconazole Nitrate (2.99)	Triamcinolone (2.38)
16	Promazine hydrochloride (0.97)	Benperidol (2.94)	Ozagrel hydrochloride (2.36)
17	Indatraline hydrochloride (0.97)	Mifepristone (2.94)	Verteporfin (2.35)
18	Chloramphenicol (0.96)	Ipsapirone (2.93)	**Vorinostat (2.30)**
19	Alprenolol hydrochloride (0.95)	Ioversol (2.92)	Oxiconazole Nitrate (2.25)
20	Flucloxacillin sodium (0.95)	Nadolol (2.87)	Halcinonide (2.20)

Figure 1. Experimental workflow and identification of vorinostat as an IFN-I inhibitor. (A) Schematic overview. (B) Compounds were evaluated to reduce IFN-I induction activity without affecting cell viability (reporter assay and cell counting kit-8). (C) Top 20 compounds from screening showed potent IFN-I inhibition with maintained viability. (D) Dose-dependent IFN-I inhibition by vorinostat. THP1-Blue ISG cells were stimulated with LPS (500 ng/mL), 2'3'-cGAMP (5 μg/mL), and R848 (5 μg/mL). ISG-inducing activity (SEAP assay) decreased with vorinostat. (E) Validation using in PBMCs (same stimuli). IFN-I activity (SEAP assay) decreased with vorinostat. Data represent the mean ± SEM from duplicate measurements across three independent experiments. IFN, interferon; LPS, lipopolysaccharide; NZB/W F1, New Zealand Black/White F1; PBMC, peripheral blood mononuclear cell; SAVI, STING-associated vasculopathy with onset in infancy; SEAP, secreted embryonic alkaline phosphatase; SLE, systemic lupus erythematosus.

Vorinostat improves interferonopathy in SAVI model mice. To investigate the therapeutic effect of vorinostat, we first analyzed the in vivo concentration of vorinostat in serum, spleen, and liver at 15 minutes, 1 hour, 2 hours, 4 hours, 8 hours, and 24 hours after intraperitoneal administration of vorinostat (20 mg/kg) by LC-MS. We found that serum vorinostat levels were >20 μM at 15 minutes and rapidly dropped to approximately 0.5 μM at one hour after administration. Similar dynamics were also observed in the spleen. However, vorinostat was detected at lower levels in the liver 15 minutes after administration, likely due to metabolism (Figure 3A). Under physiologic conditions, vorinostat concentration decreased relatively quickly, but we investigated the therapeutic effect of vorinostat on IFN-I–related disease in a mouse model of SAVI (N153S), a rare human autoinflammatory disease. SAVI mice have lung fibrosis and interstitial kidney damage because the N153S mutation of STING constitutively activates the cGAS-STING pathway, resulting in IFN-I overproduction.[28,29] We administered vorinostat (20 mg/kg) intraperitoneally for eight weeks to mitigate disease severity in SAVI mice by evaluating lung inflammation, fibrosis, serum IFN-I levels, and interstitial kidney damage (n = 7 per group). Histologic analysis of lung tissues revealed that vorinostat treatment significantly reduced pulmonary inflammation and fibrosis in SAVI mice (Figure 3B). Additionally, vorinostat improved serum IFN-I levels (Figure 3C) and reduced *N*-acetylglucosaminidase values, an indicator of interstitial nephritis (Figure 3D). Furthermore, we analyzed the expression of inflammatory cytokines and IFN-I–related genes in the lungs and kidneys of SAVI mice. Vorinostat-treated SAVI mice showed decreased expression of *Tnf*, *Il6*, and *Cxcl10* in the lung and *Ifnb1*, *Tmem173*, and *Irf3* in the kidney (Figure 3E). These results suggest vorinostat can improve disease severity by suppressing IFN-I–related signaling, despite its short half-life in vivo.

Vorinostat suppresses PC differentiation with differential effects on IFN-I production. In SLE, autoantibodies are produced by antibody-secreting cells (ASCs) such as DNB cells, short-lived plasmablasts that proliferate in response to TLR7 signaling.[10] We showed that vorinostat impedes IFN-I production via TLR7-mediated signaling. Therefore, we examined vorinostat effects on human B cell differentiation into PCs. We isolated B cells from healthy individuals and patients with SLE and cultured them with a combination of stimuli to promote PC differentiation.[10] The effect of vorinostat on B cell differentiation was assessed by flow cytometry (Figure 4A). Vorinostat curtailed the differentiation of B cells into PCs in healthy individuals and patients with SLE (detailed patient characteristics are provided in Supplementary Table S5) (Figure 4B and 4C). Next, we investigated the involvement of TBK1 and IFN-I in the differentiation of ASCs using GSK8612, a TBK1 inhibitor, and anifrolumab, an anti-IFNAR1–neutralizing antibody. Neither GSK8612 nor anifrolumab suppressed PC differentiation (Figure 4D), suggesting that vorinostat directly inhibits ASC differentiation. To further elucidate the mechanism underlying the suppression of PC differentiation, we identified the critical period of TLR-7 signaling for PC differentiation by evaluating the expression of *Prdm1*, *XBP1*, and *IRF4*, essential transcription factors for PC differentiation. We found that R848 administration in the first three days was required for ASC differentiation (Supplementary Figure S3). Consistently, vorinostat administration in the early stage of PC differentiation significantly suppressed the expression of these genes (Figure 4E), suggesting that the critical working period of vorinostat is similar to that of TLR7 signaling for PC differentiation. Additionally, vorinostat suppressed IgG production by inhibiting PC differentiation (Figure 4F). Of note, there was no remarkable suppression of IgG secretion when vorinostat was added in the late phase of PC differentiation, suggesting that vorinostat acts in the early phase of PC differentiation. Furthermore, vorinostat suppressed the production of anti–double-stranded DNA (dsDNA) antibodies by B cells from patients with SLE (Figure 4H).

Vorinostat improves survival rate and nephritis by inhibiting IFN-I production and aberrant B cell maturation. Next, we elucidated the physiologic efficacy of vorinostat in SLE-prone mice using NZB/W F1 mice, which show glomerulonephritis, elevated autoantibody titer, and low complement (C3) due to enhanced IFN-I levels and extrafollicular B cell differentiation.[30] First, we conducted the intermediate-dose administration protocol and monitored survival and proteinuria. Vorinostat (20 mg/kg) was intraperitoneally administered to 22-week-old female NZB/W F1 mice five times per week for 16 weeks. Vorinostat improved survival and reduced the frequency of ≥2 proteinuria-positive mice as quantitatively assessed using a urine tape (Figure 5A and 5B). Additionally, vorinostat significantly improved disease activity markers, including serum C3 levels, anti-dsDNA antibody titers, and urinary protein levels (Figure 5C). Next, we conducted a high-dose administration protocol to shorten the evaluation period by administering a higher dose of vorinostat (40 mg/kg) daily to 25-week-old female NZB/W F1 mice for 4 weeks. Vorinostat ameliorated glomerulonephritis (Figure 5D) and reduced the deposition of IgM, IgG, and C3 within the glomeruli (Figure 5E). Consistently, serum IFN-I levels and expression of IFN-I–related genes, such as *Tlr7*, *Mx1*, and *Ifi44*, in the spleen and bone marrow were reduced in vorinostat-treated mice (Figure 5F and 5G). Additionally, the number of pDCs in the spleen and B cells, especially mature B cells, and the percentage of ABCs in B cells in the spleen was reduced in vorinostat-treated mice (Figure 5H, 5I, and 5J). In the bone marrow, the number of pre-B cells, but not pro-B cells, was reduced by vorinostat treatment (Figure 5K), and the expression of *Vpreb1*, which encodes the surrogate BCR and is involved in the pre-B cell expansion, was considerably reduced in vorinostat-treated mice (Figure 5L), suggesting that vorinostat impaired B cell transition from pro-B cells to pre-B cells. On the other hand, vorinostat treatment did not affect T cell proportions in the spleen (Supplementary

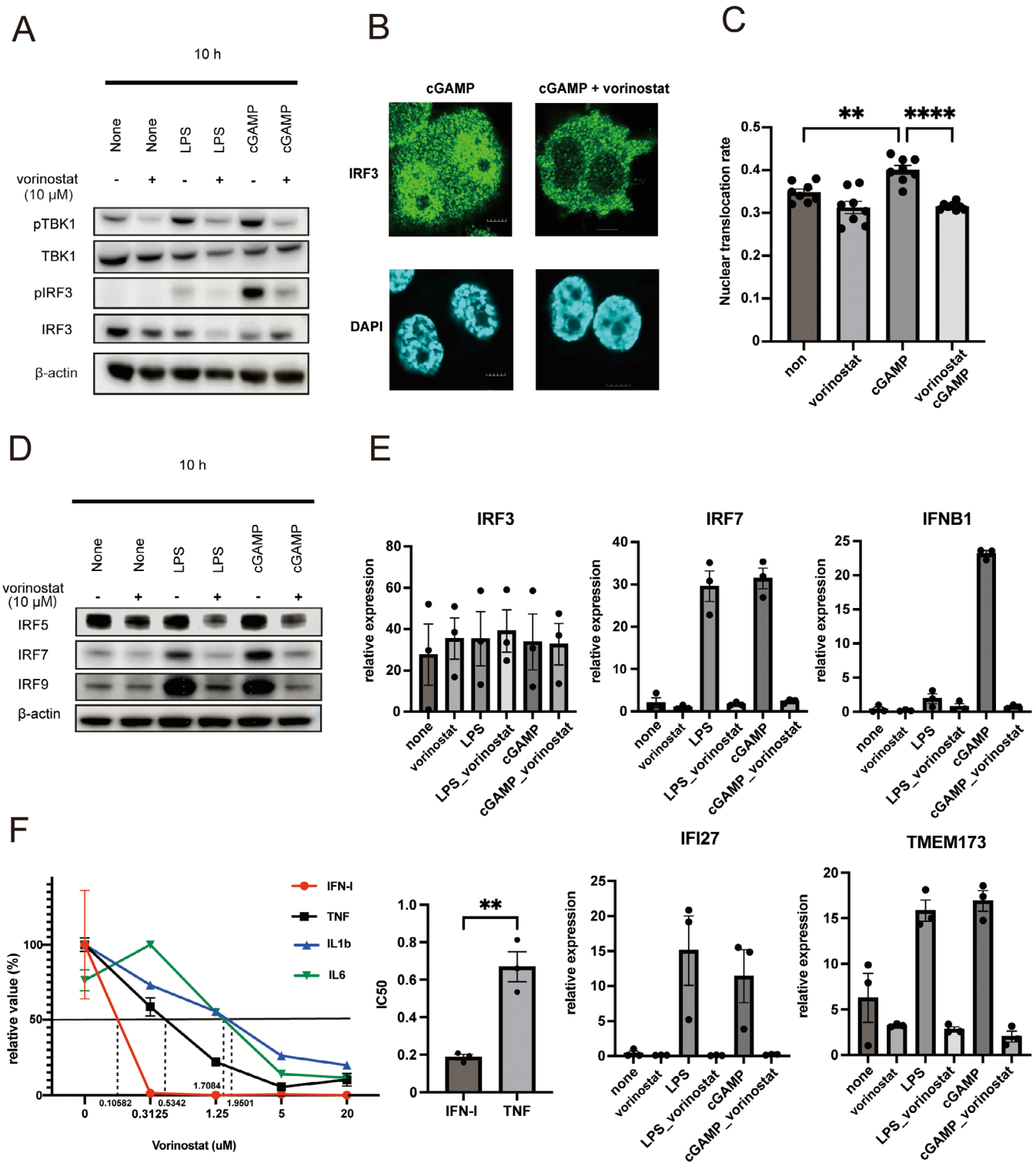

Figure 2. Vorinostat inhibits TBK1/IRF3 phosphorylation and IRF expression. THP1 cells were treated with vorinostat, followed by stimulation with LPS (500 ng/mL) and 2'3'-cGAMP (5 μg/mL) for 10 hours. (A) Western blot analysis demonstrates that vorinostat suppresses the phosphorylation of TBK1 and IRF3. (B and C) Immunofluorescence analysis reveals that vorinostat inhibits the nuclear translocation of IRF3 following cGAMP stimulation (scale bar: 5 μm). (D) Western blotting shows that vorinostat reduces the expression of IRF5, IRF7, and IRF9, contributing to the attenuation of the IFN-I response. (E) Quantitative polymerase chain reaction analysis showed that vorinostat treatment suppresses multiple IFN-I–related genes (*IRF7*, *IFNb*, *IFI27*, and *TMEM173*), without affecting *IRF3* expression. (F) Comparative analysis of the inhibitory effects of vorinostat. The 50% inhibition concentration values for suppression of different cytokines in LPS (500 ng/mL)–stimulated cells were determined by reporter assay and enzyme-linked immunosorbent assay. Data represent the mean ± SEM of duplicate or triplicate measurements from a representative of three independent experiments. IFN, interferon; LPS, lipopolysaccharide. Color figure can be viewed in the online issue, which is available at http://onlinelibrary.wiley.com/doi/10.1002/art.43434/abstract.

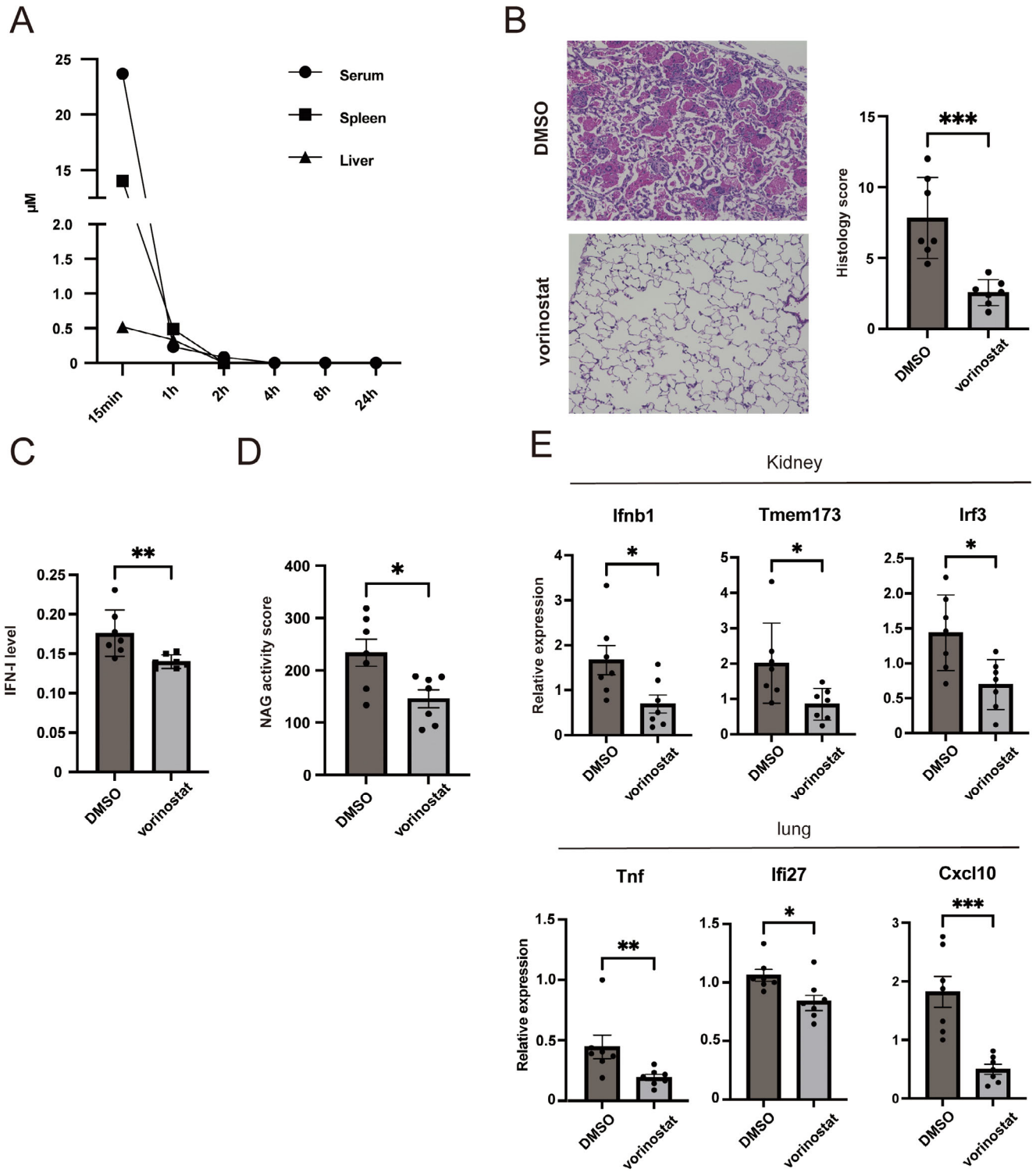

Figure 3. Vorinostat ameliorates disease phenotypes in STING-associated vasculopathy with onset in infancy mice. (A) Pharmacokinetic analysis of vorinostat in C57BL/6J mice following single intraperitoneal administration (20 mg/kg). Mice were intraperitoneally administered vorinostat (20 mg/kg) once daily for eight weeks. (B) Lung tissue sections stained with Azan from both vorinostat-treated and control mice, with a quantifiable reduction in histology scores that indicate disease severity (scale bar: 100 μm). (C) Serum IFN-I levels, assessed using the B16-Blue IFN-αβ reporter assay, were significantly reduced in the vorinostat-treated group, demonstrating the efficacy of the drug in moderating IFN-I overproduction. (D) The urinary activity of *N*-acetyl-beta-D-glucosaminidase, a marker of interstitial renal damage, was decreased in the vorinostat group, indicating improved renal function. (E) Quantitative real-time polymerase chain reaction analysis of lung and kidney tissues revealed down-regulation of IFN-I–related and inflammatory gene expression in mice treated with vorinostat. Data are presented as mean ± SEM; $^{*}P < 0.05$, $^{**}P < 0.01$, and $^{***}P < 0.001$, denoting different levels of significance. IFN, interferon. Color figure can be viewed in the online issue, which is available at http://onlinelibrary.wiley.com/doi/10.1002/art.43434/abstract.

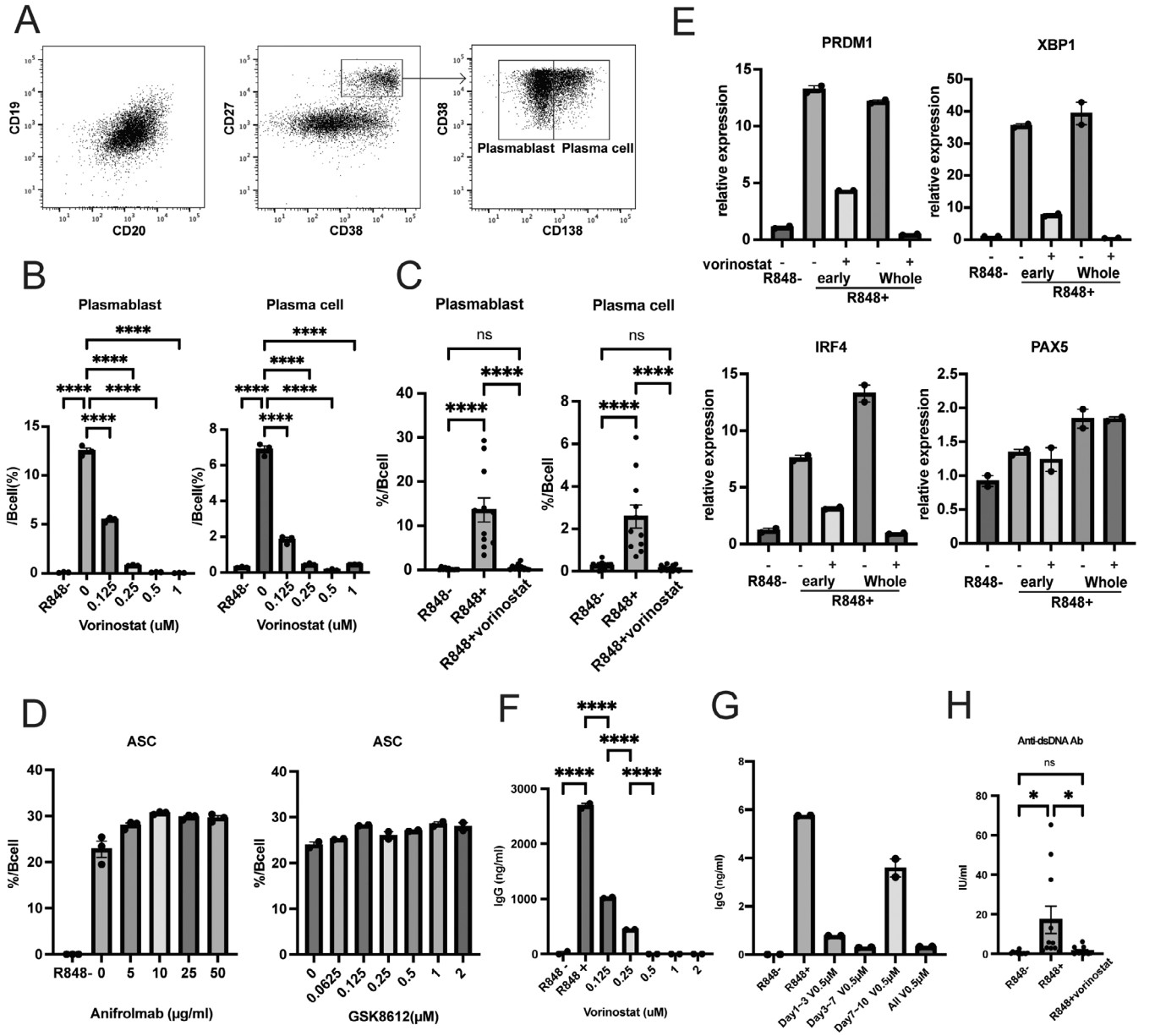

Figure 4. Vorinostat inhibits plasma cell differentiation and suppresses plasma cell–associated transcription factors. (A) Gating strategy for plasmablasts and plasma cells. Plasmablasts were defined as CD19+CD27+CD38+CD138– cells; plasma cells were defined as CD19+CD27+-CD38+CD138+ cells. (B) Vorinostat impedes the transition of human B cells to plasma cells. The percentage of plasmablasts and plasma cells was determined by fluorescence-activated cell sorting. (C) Vorinostat suppress in vitro B cell differentiation to ASC in patients with systemic lupus erythematosus. B cells isolated from patients with systemic lupus erythematosus (n = 11) were cultured with 0.5 μM vorinostat. (D) Anifrolumab does not inhibit ASC differentiation. (E) Vorinostat inhibited the expression of key plasma cell transcription factors *Prdm1*, *XBP1*, and IRF4. (F) Vorinostat dose-dependently suppressed IgG production. IgG levels in culture supernatants were measured by enzyme-linked immunosorbent assay. (G) Early or intermediate phase treatment with vorinostat is crucial for IgG secretion. Vorinostat (0.5 μM) was added at different phases: days 1 to 3 (early phase), days 3 to 7 (intermediate phase), or days 7 to 10 (late phase). (H) Vorinostat suppresses the production of anti-dsDNA antibodies (n = 11). Data are expressed as mean ± SEM of three independent experiments, with duplicate or triplicate wells per experiment. $^{*}P < 0.05$, $^{**}P < 0.01$, $^{*}P < 0.001$. Ab, antibody; ASC, antibody-secreting cell; dsDNA, double-stranded DNA. ns, not significant.

Figure S4A). Consistently, one week of vorinostat administration to healthy C57BL/6 mice did not affect these specific pathways (Supplementary Figure S4B). These results indicate that vorinostat improves survival and glomerulonephritis in lupus-prone NZB/W F1 mice by inhibiting IFN-I–related signaling and B cell differentiation by suppressing pathologic immune cells in SLE such as pDCs and ABCs, without affecting the T cell population.

Evaluation of other HDAC inhibitors for IFN-I production and PC differentiation. Because vorinostat is a

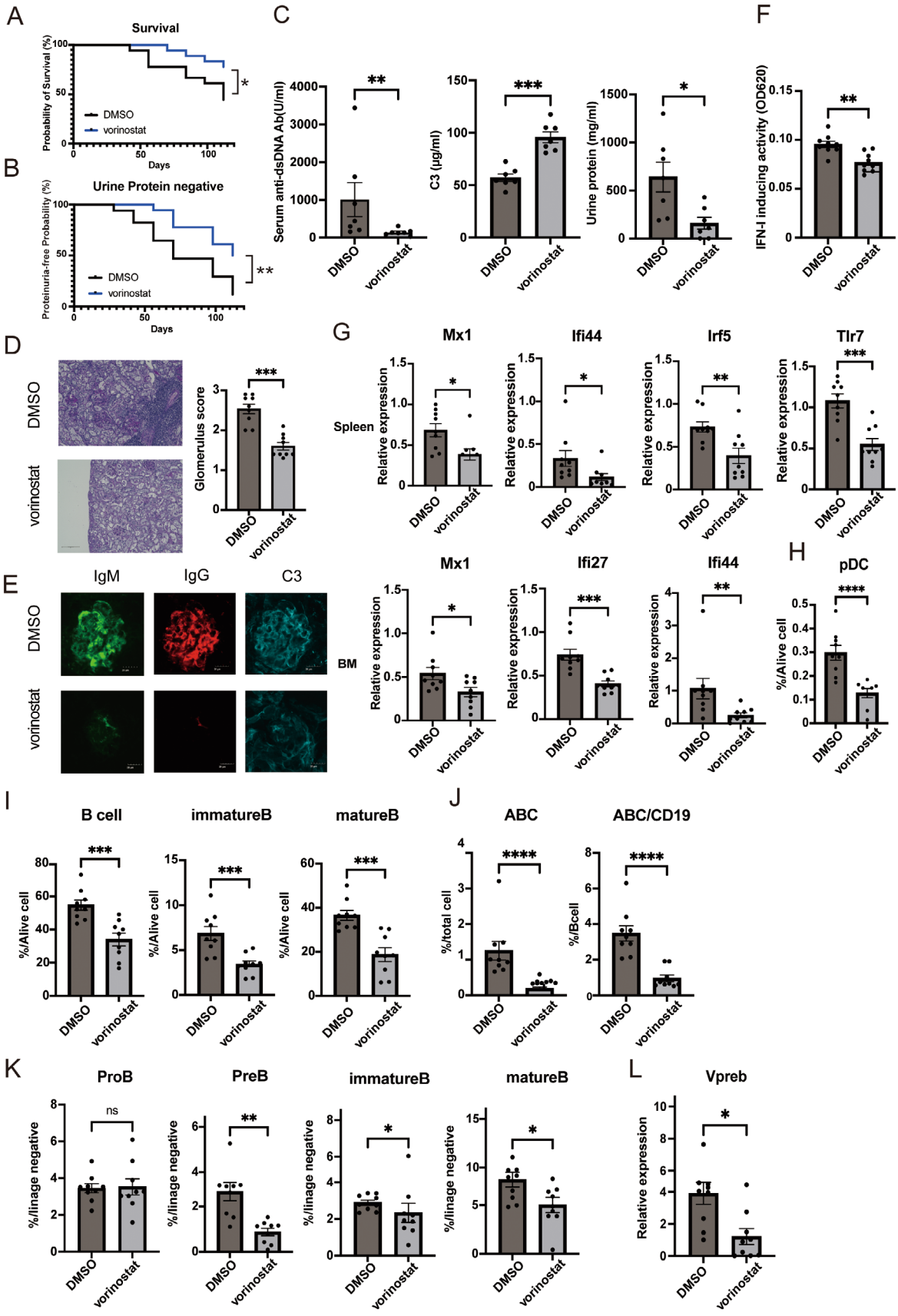

Figure 5. Legend on next page.

pan-HDAC inhibitor, we evaluated the HDAC class underlying IFN-I production and PC differentiation. We compared vorinostat with selective HDAC inhibitors, including those for HDAC1, HDAC2, HDAC3, and HDAC6, and the specific TBK1 inhibitor GSK8612. First, we evaluated the inhibitory effect of ISG induction using THP1-ISG cells with LPS, cGAMP, or R848. ISG induction was suppressed by HDAC6 inhibitors, as well as by vorinostat and TBK1 inhibitors, but not by HDAC1 and HDAC2 inhibitors (Supplementary Figure S5A). Then, we evaluated cytokine production from human PBMCs and found that HDAC1 and HDAC2 inhibitors did not inhibit the production of IFN-I, TNF-α, and IL-6, but HDAC6 inhibitors, as well as vorinostat, suppressed them (Figure 6A and 6B). Consistently, similar to vorinostat and the TBK1 inhibitor, the HDAC6 inhibitor was able to suppress TBK1 phosphorylation and IRF7 and IRF9 expression (Supplementary Figure S5B). The HDAC3 inhibitor partially suppressed IFN-I production but did not suppress TNF-α and IL-6 production (Figure 6A and 6B). Notably, simultaneous inhibition of HDAC3 and HDAC6 suppressed IFN-I levels comparable to those observed with vorinostat, suggesting that HDAC3 and HDAC6 may act synergistically to regulate IFN-I signaling (Supplementary S5C). In contrast, HDAC6 inhibitor, but not HDAC3 inhibitor, significantly impaired B cell differentiation into PCs (Figure 6C), suggesting that HDAC6 may be involved in both IFN-I production and PC differentiation. Finally, we evaluated different clinically approved pan-HDAC inhibitors, including panobinostat, chidamide, romidepsin, and belinostat. Similar to vorinostat, all HDAC inhibitors suppressed PC differentiation to varying degrees. Nonetheless, the inhibitory effect on IFN-I production differed, with romidepsin and belinostat inhibiting IFN-I but not panobinostat and chidamide (Figure 6D). Although some kinds of HDAC inhibitors may inhibit IFN-I production and PC differentiation, the underlying mechanisms may differ according to the drug.

DISCUSSION

SLE is a systemic autoimmune disease characterized by a breakdown of innate and acquired immune tolerance, leading to increased production of IFN-I and autoantibodies against DNA- and RNA-associated antigens. Multiple pathways contribute to aberrant B cell differentiation in SLE, with TLR7 signaling being a key mechanism driving disease progression. Recently, autoreactive B cells have been shown to undergo extrafollicular development to become antibody-producing cells by DNB cells, correlating with SLE disease activity.[10,31] This process can be initiated through various pathways, including both BCR stimulation by binding to extracellular DNA and/or RNA and TLR7/9 stimulation by antibody-mediated DNA and/or RNA internalization. Small cytoplasmic RNA-seq analysis revealed that the B cell subcluster increases in patients with SLE expressing DNB-related genes, including TBX21, ITGAX, and IL10, with high levels[32] of TLR7. We showed that vorinostat inhibits TBK1 and IRF3 phosphorylation induced by TLR ligands, including TLR7, or STING activation, reducing IRF5, IRF7, and IRF9 expression. Furthermore, vorinostat prevents TLR7-mediated PC differentiation by suppressing key transcription factors essential for PC development, including Prdm1, XBP1, and IRF4. Thus, vorinostat is a promising candidate for treating SLE because it inhibits both IFN-I production and abnormal B cell maturation, which are abnormally up-regulated in SLE.

HDACs play dual roles in the cytosol and the nucleus. In the cytosol, HDAC3 was reported to promote IFN-I production by triggering TBK1 deacetylation and subsequent phosphorylation.[24] HDAC6 is a deacetylase enzyme that targets histone proteins in the nucleus and cytoplasmic proteins such as α-tubulin and HSP90 in the cytoplasm and is involved in NLRP3 inflammasome activation, NF-κB p65 expression, and autophagy induction.[33–35] HDAC6 positively regulates NF-κB signaling by promoting IκBα degradation and p65 nuclear translocation, whereas HDAC6 inhibition increases p65 acetylation and reduces inflammatory response.[36,37] HDAC6 activates IRF3 via deacetylation of RIG-I and modulates phosphorylation of STAT1 through acetylation of STAT1 itself,[38,39] suggesting that HDAC6 influences both upstream and downstream components of the IFN-I pathway.

Additionally, nuclear HDAC6 regulates the transcription of genes related to NF-kB and IRFs. HDAC6 interacts with p65/RelA, a NF-κB subunit, that inhibits p65 binding to the target promoters through deacetylation, thereby repressing NF-κB–driven gene transcription.[40] In a PKCα–β-catenin signaling axis, HDAC6 facilitates IRF3 binding to ISG promoters by modulating acetylation status of β-catenin.[41] Thus, HDAC6 may contribute to the transcriptional regulation of NF-κB– and IRF3-related genes via chromatin remodeling, which may explain the suppression of ISG expression in our study.

Figure 5. Therapeutic effects of vorinostat through IFN-I suppression in New Zealand Black/White F1 lupus-prone mice. Effects of vorinostat (20 mg/kg, intraperitoneal, five times/week for 16 weeks) in New Zealand Black/White F1 mice. (A) Kaplan–Meier survival curves show improved survival in the vorinostat-treated group (log-rank test, $P = 0.0359$). (B) Reduced proteinuria scores (log-rank test, $P = 0.0087$). (C) Improvement in serum anti-dsDNA antibody titers, C3 levels, and proteinuria (n = 7 per group). (D) Decreased histopathological scores of nephritis. (E) Reduced glomerular deposition of IgM, IgG, and C3 by immunofluorescence analysis. (F) Decreased serum IFN-I levels measured by B16-Blue IFN-α/β reporter cells. (G) Vorinostat suppresses IFN-I–related gene expression in the spleen and bone marrow. (H) Vorinostat reduced the number of splenic pDCs. (I) Vorinostat decreased the number of B cells in the spleen. (J) Vorinostat decreased the percentage of ABCs among B cells in the spleen. (K) Vorinostat treatment reduced the number of pre-B cells but did not affect pro-B cells. (L) Suppressed Vpreb1 expression in bone marrow B cells. Data are expressed as mean ± SEM; $^{*}P < 0.05$, $^{**}P < 0.01$, and $^{***}P < 0.001$. ABC, age-associated B cell; dsDNA, double-stranded DNA; IFN, interferon; pDC, plasmacytoid dendritic cell. Color figure can be viewed in the online issue, which is available at http://onlinelibrary.wiley.com/doi/10.1002/art.43434/abstract.

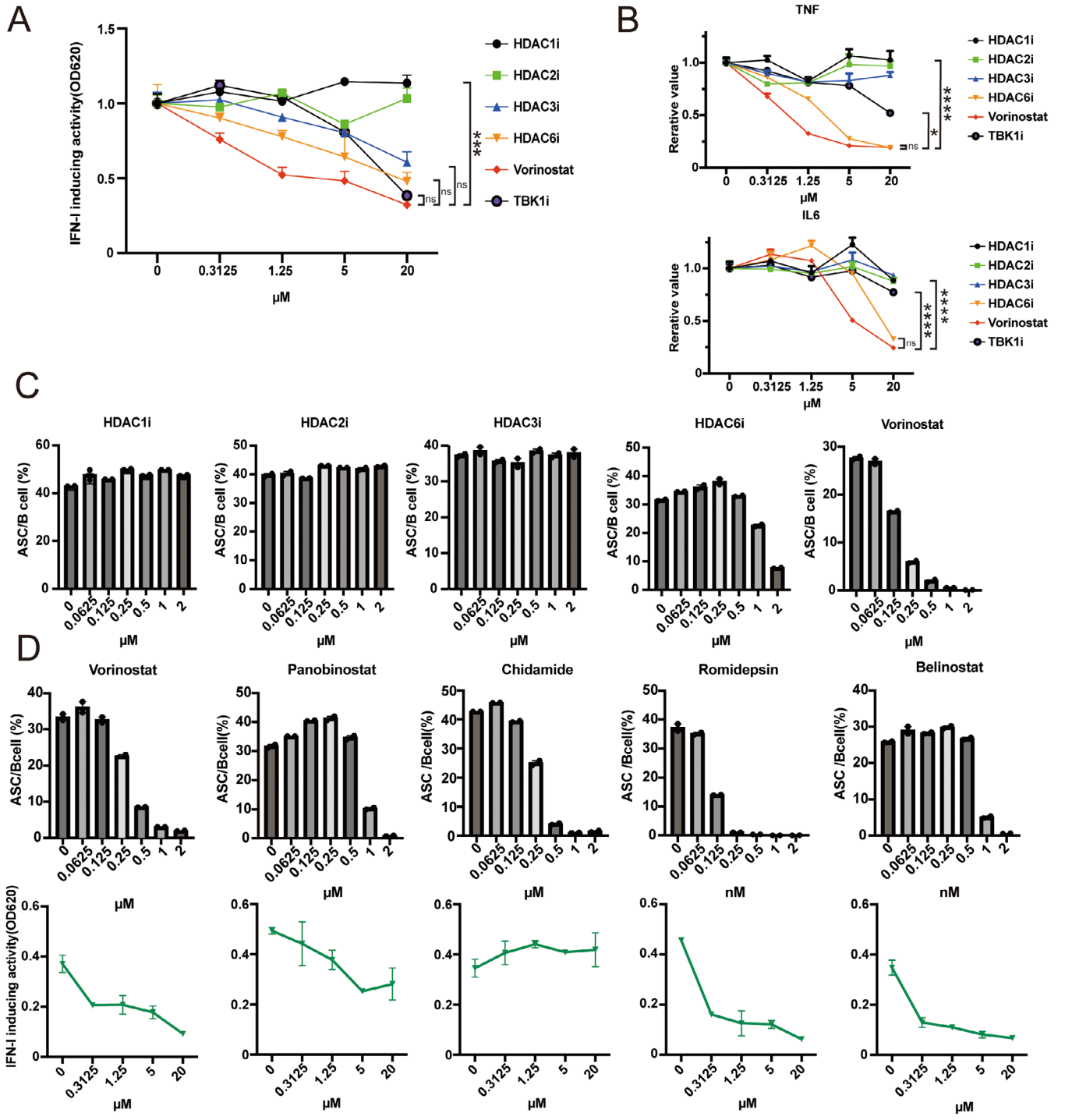

Figure 6. Evaluation of other HDAC inhibitors for IFN-I production and plasma cell differentiation. (A, B) Proinflammatory cytokine production (IFN-I, TNF-α, IL-6) in PBMCs stimulated with R848 (2.5 μg/mL) and treated with selective HDAC inhibitors targeting HDAC1, HDAC2, HDAC3, HDAC6, TBK1 inhibitor (GSK8612), or vorinostat. (A) IFN-I bioactivity was measured by HEK-Blue IFN-α/β reporter cells. (B) TNF-α and IL-6 concentration were measured by enzyme-linked immunosorbent assay. Statistical significance of other compounds against vorinostat was evaluated by one-way analysis of variance (*$P < 0.05$, ***$P < 0.001$, ****$P < 0.0001$). (C) Plasma cell differentiation assay under plasmablast-inducing conditions with selective HDAC inhibitors. The percentage of ASC per B cells was evaluated by fluorescence-activated cell sorting. (D) Effects of clinically approved HDAC inhibitors (vorinostat, panobinostat, chidamide, romidepsin, and belinostat) on human ASC differentiation (upper) and IFN-I production in PBMCs (lower). B cells were cultured seven days with inhibitors. PBMCs were stimulated with R848 (2.5 μg/mL) for 24 hours with inhibitors. IFN-I activity in supernatants was measured. Data are expressed as mean ± SEM of three independent experiments. ASC, antibody-secreting cell; HDAC, histone deacetylase; IL, interleukin; IFN, interferon; ns, not significant; PBMC, peripheral blood mononuclear cell. Color figure can be viewed in the online issue, which is available at http://onlinelibrary.wiley.com/doi/10.1002/art.43434/abstract.

We demonstrated mild suppression of IFN-I production by selective HDAC3 inhibition in PBMCs and the involvement of HDAC6 in IFN-I production through the phosphorylation of TBK1 and the expression of IRF7 and IRF9. The experiments using HDAC-specific inhibitors showed that HDAC6 and HDAC3 additively regulated IFN-I production. However, HDAC6 was involved in TBK1 phosphorylation induced by LPS and cGAMP stimulation in THP1 cells, whereas HDAC3 was not involved, suggesting that the mode of function for HDAC6 and HDAC3 may be different according to the activation state; therefore, the differences between our observations and previous reports are likely due to differences in experimental settings.

Epigenetic dysregulation, particularly histone hypoacetylation, has been implicated in SLE pathogenesis. Specifically, hypoacetylation of histones H3 and H4 in B cells alters the expression of immune response–related genes in patients with SLE and in lupus-prone mice. Previous studies with HDAC inhibitors showed therapeutic potential in lupus models.[42,43] Thus, epigenetic control by HDAC inhibitors may be a promising strategy for the treatment of SLE. We showed that vorinostat improves mortality and disease severity by suppressing in vivo IFN-I production and ASC differentiation in lupus-prone mice. Moreover, vorinostat's mechanisms of action were similar to those of HDAC6 selective inhibitors, suggesting that vorinostat may exert its effects mainly through HDAC6 inhibitory activity.

Vorinostat is clinically approved for cutaneous T cell lymphoma, with well-characterized pharmacokinetics and side effect profiles. Conventional drugs have limited efficacy due to their broad or highly limited immunologic effects. Glucocorticoids inhibit the NF-κB pathway, thereby suppressing the production of inflammatory cytokines and antibodies, but they cannot inhibit IFN-I signal transduction and are associated with a wide range of side effects. Hydroxychloroquine selectively suppresses IFN-α production via TLR7/9 inhibition in pDCs but has little effect on B cells.[44] Belimumab primarily targets B cells, attenuating the differentiation of autoantibody-producing plasmablasts with only minimal direct effects on IFN-I pathways.[45] This mechanistic distinction underscores the therapeutic value of vorinostat and provides a foundation for its potential in SLE. Thus, it is essential to optimize key parameters such as dosage, route of administration, targeted delivery, and molecular editing to maximize the clinical efficacy and minimize side effects of vorinostat.

Clinical adverse effects of vorinostat include infection, thrombocytopenia, and liver damage. Vorinostat decreased the mRNA levels of glycolytic enzymes such as lactate dehydrogenase and mitotic checkpoint regulators including *KNL1* and *APC/C* in human PBMCs. Glycolysis-derived metabolites support T cell proliferation by providing critical substrates for histone acetylation and epigenetic remodeling during early activation.[46] Similarly, activated B cells up-regulate glycolytic enzyme to support clonal expansion and PC differentiation via germinal center B cells.[47] On the other hand, KNL1 and APC/C are involved in cell division and proliferation by regulating cell cycle progression. Therefore, dysfunction of these enzymes might lead to metabolic reprogramming and lymphocyte proliferation disorders following vorinostat administration.[48] Furthermore, the long-term effects of sustained histone acetylation induced by vorinostat are another concern. HDAC6-deficient mice were reported to exhibit no gross developmental or baseline immunologic abnormalities, apart from augmented regulatory T cell function, under physiologic conditions.[49,50] We showed that vorinostat-treated mice were healthy, with no effect on T cell populations, anorexia, weight loss, and little off-target expression or repression of mRNAs, suggesting to be tolerable for SLE. Of note, serum and spleen vorinostat levels decreased below the effective blood concentration (>500 nM) within two hours after administration,[51] similar to that in humans. The rapid clearance of vorinostat may contribute to reduced adverse effects in mice. Despite this short half-life, it is noteworthy that vorinostat demonstrated significant therapeutic effects for SLE-prone mice.

Study limitations include the following: (1) the number of mice and PBMCs from patients with SLE were insufficient; daily intraperitoneal administration due to the short half-life of the drug was necessary. Therefore, the translational extension of these findings to humans must be considered with caution. (2) The effects of vorinostat on other immune cells have not yet been investigated. It is necessary to clarify the effects of long-term histone acetylation by HDAC inhibitors on immune memory responses. (3) The influence of vorinostat on other cellular functions such as metabolism and proliferation have not been fully elucidated. Sustained inhibition of genes associated with metabolism and mitosis may impair the accuracy of chromosome segregation, highlighting the importance of long-term safety monitoring. (4) The exact molecular mechanisms by which vorinostat and HDAC6 inhibitor suppresses IFN-I production and PC differentiation remain unclear. Future studies, including multiomics approaches such as assay for transposase-accessible chromatin with high-throughput sequencing and chromatin immunoprecipitation sequencing, will be important for dissecting the epigenetic and transcriptional changes underpinning inhibition of IFN-I signaling and B cell maturation.

In conclusion, our findings show that vorinostat improved SLE symptoms in mice by simultaneously suppressing pathologic IFN-I production and aberrant B cell differentiation, primarily targeting HDAC6. Vorinostat and other HDAC inhibitors should be reevaluated as promising therapeutic agents for SLE, offering more effective and well-tolerated solutions for patients with SLE.

ACKNOWLEDGMENTS

We acknowledge the next-generation sequencing core facility at the Research Institute for Microbial Diseases of Osaka University for the sequencing and data analysis. We are also grateful to the members of animal facility in Osaka University for maintaining the mice.

AUTHOR CONTRIBUTIONS

All authors contributed to at least one of the following manuscript preparation roles: conceptualization AND/OR methodology, software, investigation, formal analysis, data curation, visualization, and validation AND drafting or reviewing/editing the final draft. As corresponding author, Dr Takamatsu confirms that all authors have provided the final approval of the version to be published and takes responsibility for the affirmations regarding article submission (eg, not under consideration by another journal), the integrity of the data presented, and the statements regarding compliance with institutional review board/Declaration of Helsinki requirements.

REFERENCES

1. Kato Y, Park J, Takamatsu H, et al. Apoptosis-derived membrane vesicles drive the cGAS-STING pathway and enhance type I IFN production in systemic lupus erythematosus. Ann Rheum Dis 2018;77(10):1507–1515.
2. Gupta S, Kaplan MJ. Bite of the wolf: innate immune responses propagate autoimmunity in lupus. J Clin Invest 2021;131(3):e144918.
3. Banchereau R, Hong S, Cantarel B, et al. Personalized immunomonitoring uncovers molecular networks that stratify lupus patients. Cell 2016;165(6):1548–1550.
4. Itotagawa E, Tomofuji Y, Kato Y, et al. SLE stratification based on BAFF and IFN-I bioactivity for biologics and implications of BAFF produced by glomeruli in lupus nephritis. Rheumatology (Oxford) 2023;62(5):1988–1997.
5. Banchereau J, Pascual V. Type I interferon in systemic lupus erythematosus and other autoimmune diseases. Immunity 2006;25(3):383–392.
6. Muskardin TLW, Niewold TB. Type I interferon in rheumatic diseases. Nat Rev Rheumatol 2018;14(4):214–228.
7. Akira S, Uematsu S, Takeuchi O. Pathogen recognition and innate immunity. Cell 2006;124(4):783–801.
8. Heinz LX, Lee J, Kapoor U, et al. TASL is the SLC15A4-associated adaptor for IRF5 activation by TLR7-9. Nature 2020;581(7808):316–322.
9. Feng D, Stone RC, Eloranta ML, et al. Genetic variants and disease-associated factors contribute to enhanced interferon regulatory factor 5 expression in blood cells of patients with systemic lupus erythematosus. Arthritis Rheum 2010;62(2):562–573.
10. Jenks SA, Cashman KS, Zumaquero E, et al. Distinct effector B cells induced by unregulated Toll-like receptor 7 contribute to pathogenic responses in systemic lupus erythematosus. Immunity 2018;49(4):725–739.e6.
11. Sakata K, Nakayamada S, Miyazaki Y, et al. Up-regulation of TLR7-mediated IFN-α production by plasmacytoid dendritic cells in patients with systemic lupus erythematosus. Front Immunol 2018;9:1957.
12. Shapiro-Shelef M, Calame K. Regulation of plasma-cell development. Nat Rev Immunol 2005;5(3):230–242.
13. Reimold AM, Iwakoshi NN, Manis J, et al. Plasma cell differentiation requires the transcription factor XBP-1. Nature 2001;412(6844):300–307.
14. Klein U, Casola S, Cattoretti G, et al. Transcription factor IRF4 controls plasma cell differentiation and class-switch recombination. Nat Immunol 2006;7(7):773–782.
15. Lam JH, Baumgarth N. Toll-like receptor mediated inflammation directs B cells towards protective antiviral extrafollicular responses. Nat Commun 2023;14(1):3979.
16. Rubtsova K, Rubtsov AV, Cancro MP, et al. Age-associated B cells: a T-bet-dependent effector with roles in protective and pathogenic immunity. J Immunol 2015;195(5):1933–1937.
17. Rubtsova K, Marrack P, Rubtsov AV. TLR7, IFNγ, and T-bet: their roles in the development of ABCs in female-biased autoimmunity. Cell Immunol 2015;294(2):80–83.
18. Siegel D, Hussein M, Belani C, et al. Vorinostat in solid and hematologic malignancies. J Hematol Oncol 2009;2(1):31.
19. Hochberg MC. Updated American College of Rheumatology revised criteria for the classification of systemic lupus erythematosus. Arthritis Rheum 1997;40(9):1725. https://doi.org/10.1002/art.1780400928
20. Motwani M, Pawaria S, Bernier J, et al. Hierarchy of clinical manifestations in SAVI N153S and V154M mouse models. Proc Natl Acad Sci USA 2019;116(16):7941–7950.
21. Temizoz B, Shibahara T, Hioki K, et al. 5,6-dimethylxanthenone-4-acetic acid (DMXAA), a partial STING agonist, competes for human STING activation. Front Immunol 2024;15:1353336.
22. Ge SX, Son EW, Yao R. iDEP: an integrated web application for differential expression and pathway analysis of RNA-Seq data. BMC Bioinformatics 2018;19(1):534.
23. An X, Sun X, Hou Y, et al. Protective effect of oxytocin on LPS-induced acute lung injury in mice. Sci Rep 2019;9(1):2836.
24. Bignon A, Gaudin F, Hémon P, et al. CCR1 inhibition ameliorates the progression of lupus nephritis in NZB/W mice. J Immunol 2014;192(3):886–896.
25. Honda K, Yanai H, Negishi H, et al. IRF-7 is the master regulator of type-I interferon-dependent immune responses. Nature 2005;434(7034):772–777.
26. Sun L, Wu J, Du F, et al. Cyclic GMP-AMP synthase is a cytosolic DNA sensor that activates the type I interferon pathway. Science 2013;339(6121):786–791.
27. Tang J-L, Yang Q, Xu C-H, et al. Histone deacetylase 3 promotes innate antiviral immunity through deacetylation of TBK1. Protein Cell 2021;12(4):261–278.
28. Bouis D, Kirstetter P, Arbogast F, et al. Severe combined immunodeficiency in stimulator of interferon genes (STING) V154M/wild-type mice. J Allergy Clin Immunol 2019;143(2):712–725.e5.
29. Liu Y, Jesus AA, Marrero B, et al. Activated STING in a vascular and pulmonary syndrome. N Engl J Med 2014;371(6):507–518.
30. Rubtsov AV, Rubtsova K, Fischer A, et al. Toll-like receptor 7 (TLR7)-driven accumulation of a novel CD11c^{+} B-cell population is important for the development of autoimmunity. Blood 2011;118(5):1305–1315.
31. Nündel K, Green NM, Shaffer AL, et al. Cell-intrinsic expression of TLR9 in autoreactive B cells constrains BCR/TLR7-dependent responses. J Immunol 2015;194(6):2504–2512.
32. Nehar-Belaid D, Hong S, Marches R, et al. Mapping systemic lupus erythematosus heterogeneity at the single-cell level. Nat Immunol 2020;21(9):1094–1106.
33. Tsujimoto K, Jo T, Nagira D, et al. The lysosomal Ragulator complex activates NLRP3 inflammasome in vivo via HDAC6. EMBO J 2023;42(1):e111389.
34. Chang P, Li H, Hu H, et al. The role of HDAC6 in autophagy and NLRP3 inflammasome. Front Immunol 2021;12:763831.
35. Ran J, Zhou J. Targeted inhibition of histone deacetylase 6 in inflammatory diseases. Thorac Cancer 2019;10(3):405–412.
36. Barter MJ, Butcher A, Wang H, et al. HDAC6 regulates NF-κB signalling to control chondrocyte IL-1-induced MMP and inflammatory gene expression. Sci Rep 2022;12(1):6640.
37. Xu D, Luo XM, Reilly CM. HDAC6 deletion decreases pristane-induced inflammation. Immunohorizons 2024;8(9):668–678.
38. Choi SJ, Lee HC, Kim JH, et al. HDAC6 regulates cellular viral RNA sensing by deacetylation of RIG-I. EMBO J 2016;35(4):429–442.

39. Wen Y, Ye S, Li Z, et al. HDAC6 inhibitor ACY-1215 enhances STAT1 acetylation to block PD-L1 for colorectal cancer immunotherapy. Cancer Immunol Immunother 2024;73(1):7.
40. Yang CJ, Liu YP, Dai HY, et al. Nuclear HDAC6 inhibits invasion by suppressing NF-κB/MMP2 and is inversely correlated with metastasis of non-small cell lung cancer. Oncotarget 2015;6(30):30263–30276.
41. Zhu J, Coyne CB, Sarkar SN. PKC alpha regulates Sendai virus-mediated interferon induction through HDAC6 and β-catenin. EMBO J 2011;30(23):4838–4849.
42. Garcia BA, Busby SA, Shabanowitz J, et al. Resetting the epigenetic histone code in the MRL-lpr/lpr mouse model of lupus by histone deacetylase inhibition. J Proteome Res 2005;4(6):2032–2042.
43. Regna NL, Vieson MD, Gojmerac AM, et al. HDAC expression and activity is upregulated in diseased lupus-prone mice. Int Immunopharmacol 2015;29(2):494–503.
44. Sacre K, Criswell LA, McCune JM. Hydroxychloroquine is associated with impaired interferon-alpha and tumor necrosis factor-alpha production by plasmacytoid dendritic cells in systemic lupus erythematosus. Arthritis Res Ther 2012;14(3):R155.
45. Jacobi AM, Huang W, Wang T, et al. Effect of long-term belimumab treatment on B cells in systemic lupus erythematosus: extension of a phase II, double-blind, placebo-controlled, dose-ranging study. Arthritis Rheum 2010;62(1):201–210.
46. Bailis W, Shyer JA, Zhao J, et al. Distinct modes of mitochondrial metabolism uncouple T cell differentiation and function. Nature 2019;571(7765):403–407.
47. Gracie CJ, Mitchell R, Johnstone JC, et al. The unusual metabolism of germinal center B cells. Trends Immunol 2025;46(5):416–428.
48. Doughty CA, Bleiman BF, Wagner DJ, et al. Antigen receptor-mediated changes in glucose metabolism in B lymphocytes: role of phosphatidylinositol 3-kinase signaling in the glycolytic control of growth. Blood 2006;107(11):4458–4465.
49. de Zoeten EF, Wang L, Butler K, et al. Histone deacetylase 6 and heat shock protein 90 control the functions of Foxp3(+) T-regulatory cells. Mol Cell Biol 2011;31(10):2066–2078.
50. Zhang Y, Kwon S, Yamaguchi T, et al. Mice lacking histone deacetylase 6 have hyperacetylated tubulin but are viable and develop normally. Mol Cell Biol 2008;28(5):1688–1701.
51. Giri KK, Suresh PS, Saim SM, et al. Validation of an LC-MS/MS method for simultaneous detection of four HDAC inhibitors - belinostat, panobinostat, rocilinostat and vorinostat in mouse plasma and its application to a mouse pharmacokinetic study. Biomed Chromatogr 2017;31(7):e3912.